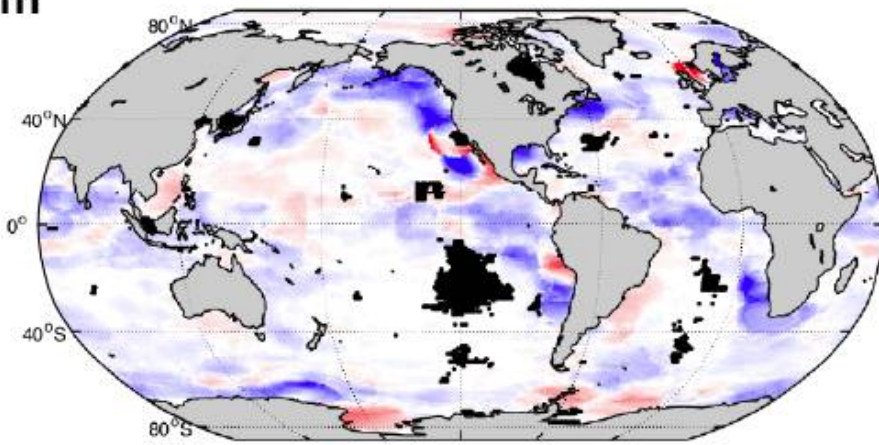


Troubling Ocean Oxygen decline

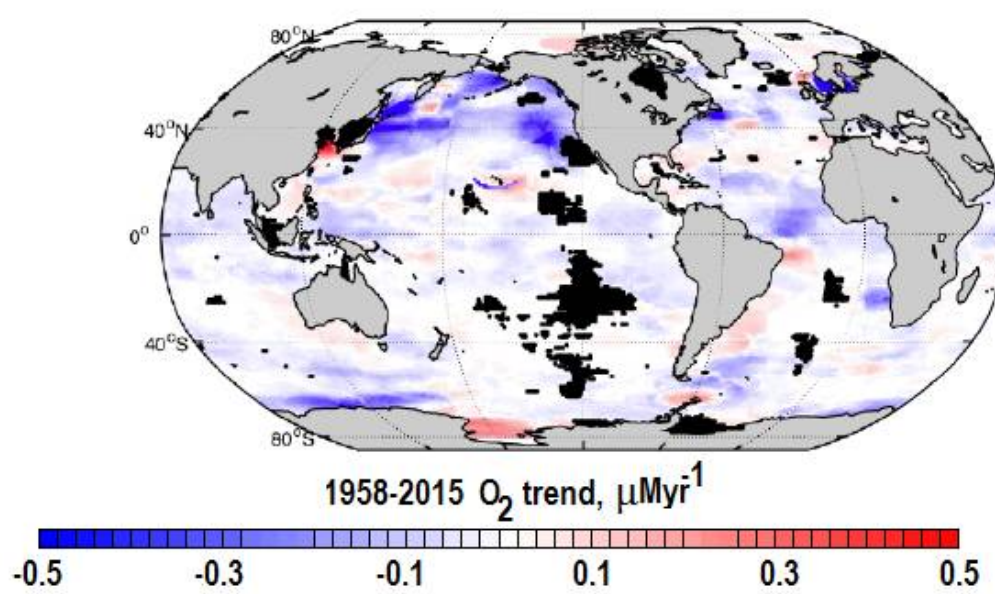
The amount of dissolved oxygen contained in the water -- an important measure of ocean health -- has been declining for more than 20 years, reveals a new analysis of decades of data (1958 to 2015) on oceans across the globe.

a. 100m



← Global map of the linear trend of dissolved oxygen.

b. 400m



A new analysis of decades of data on oceans across the globe has revealed that the amount of dissolved oxygen contained in the water -- an important measure of ocean health -- has been declining for more than 20 years.

Researchers at Georgia Institute of Technology looked at a historic dataset of ocean information stretching back more than 50 years and searched for long term trends and patterns. They found that oxygen levels started dropping in the 1980s as ocean

temperatures began to climb.

"The oxygen in oceans has dynamic properties, and its concentration can change with natural climate variability," said Taka Ito, an associate professor in Georgia Tech's School of Earth and Atmospheric Sciences who led the research. "The important aspect of our result is that the rate of global oxygen loss appears to be exceeding the level of nature's random variability."

Falling oxygen levels in water have the potential to impact the habitat of marine organisms worldwide and in recent years led to more frequent "hypoxic events" that killed or displaced populations of fish, crabs and many other organisms.

Researchers have for years anticipated that rising water temperatures would affect the amount of oxygen in the oceans, since warmer water is capable of holding less dissolved gas than colder water. But the data showed that ocean oxygen was falling more rapidly than the corresponding rise in water temperature.

The trend of oxygen falling is about two to three times faster than what we predicted from the decrease of solubility associated with the ocean warming, Ito said. This is most likely due to the changes in ocean circulation and mixing associated with the heating of the near-surface waters and melting of polar ice.

The majority of the oxygen in the ocean is absorbed from the atmosphere at the surface or created by photosynthesizing phytoplankton. Ocean currents then mix that more highly oxygenated water with subsurface water. But rising ocean water temperatures near the surface have made it more buoyant and harder for the warmer surface waters to mix downward with the cooler subsurface waters. Melting polar ice has added more freshwater to the ocean surface -- another factor that hampers the natural mixing and leads to increased ocean stratification.

After the mid-2000s, this trend became apparent, consistent and statistically significant -- beyond the envelope of year-to-year fluctuations, Ito said. "The trends are particularly strong in the tropics, eastern margins of each basin and the subpolar North Pacific.

In an earlier study, Ito and other researchers explored why oxygen depletion was more pronounced in tropical waters in the Pacific Ocean. They found that air pollution drifting from East Asia out over the world's largest ocean contributed to oxygen levels falling in tropical waters thousands of miles away.

Once ocean currents carried the iron and nitrogen pollution to the tropics, photosynthesizing phytoplankton went into overdrive consuming the excess nutrients. But rather than increasing oxygen, the net result of the chain reaction was the depletion oxygen in subsurface water.

Upper Ocean O₂ trends: 1958-2015

Takamitsu Ito¹, Shoshiro Minobe^{2,3}, Matthew C. Long⁴, and Curtis

Deutsch⁵

Taka Ito, taka.ito@eas.gatech.edu

¹Georgia Institute of Technology, Atlanta,
Georgia, USA.

²Department of Natural History Sciences,
Graduate School of Science, Hokkaido
University, Sapporo, Japan.

³Department of Earth and Planetary
Sciences, Faculty of Science, Hokkaido
University, Sapporo, Japan.

⁴Climate and Global Dynamics
Laboratory, National Center for

This article has been accepted for publication and undergone full peer review but has not been through the copyediting, typesetting, pagination and proofreading process, which may lead to differences between this version and the Version of Record. Please cite this article as doi: 10.1002/2017GL073613

Historic observations of dissolved oxygen (O_2) in the ocean are analyzed to quantify multi-decadal trends and variability from 1958 to 2015. Additional quality control is applied and the resultant oxygen anomaly field is used to quantify upper ocean O_2 trends at global and hemispheric scales. A widespread negative O_2 trend is beginning to emerge from the envelope of interannual variability. Ocean reanalysis data is used to evaluate relationships with changes in ocean heat content (OHC) and oxygen solubility ($O_{2,sat}$). Global O_2 decline is evident after the 1980s, accompanied by an increase in global OHC. The global upper ocean O_2 inventory (0-1,000m) changed at the rate of $-243 \pm 124 \text{ TmolO}_2$ per decade. Further, the O_2 inventory is negatively correlated with the OHC ($r = -0.86$; 0-1,000m) and the regression coefficient of O_2 to OHC is approximately $-8.2 \pm 0.66 \text{ nmol O}_2 \text{ J}^{-1}$, on the same order of magnitude as the simulated O_2 -heat relationship typically found in ocean climate models. Variability and trends in the observed upper ocean O_2 concentration are dominated by the Apparent Oxygen Utilization (AOU) component with relatively small contributions from $O_{2,sat}$. This indicates that changing ocean circulation, mixing and/or biochemical processes, rather than

Atmospheric Research, Boulder, Colorado,
USA.

⁵School of Oceanography, University of
Washington, Seattle, Washington, USA.

the direct thermally-induced solubility effects, are the primary drivers for the observed O₂ changes. The spatial patterns of the multi-decadal trend include regions of enhanced ocean deoxygenation including the subpolar North Pacific, eastern boundary upwelling systems and tropical oxygen minimum zones.

Further studies are warranted to understand and attribute the global O₂ trends and their regional expressions.

Keypoints:

- A widespread negative O₂ trend is beginning to emerge from the envelope of interannual variability
- The global ocean O₂ inventory is negatively correlated with the global ocean heat content
- Variability and trends in the observed upper ocean O₂ concentration are dominated by the Apparent Oxygen Utilization

1. Introduction

In this and following centuries, marine ecosystems will likely face multiple stressors as a consequence of high-CO₂ and a warming climate. The three factors—temperature increase, ocean acidification, and ocean deoxygenation—are global-scale phenomena with significant regional variations, influencing the ecosystem and biogeochemical cycles in ways not yet fully documented [Gruber, 2011]. Unraveling the nature and the consequences of these changes is one of the grand challenges for the ocean science community. The three factors are related to one another, that deoxygenation likely results in increased ocean acidification in subsurface waters. Such waters commonly supply nutrient to continental shelves, especially in upwelling regions. Thus, a better understanding of deoxygenation will improve our understanding of ocean acidification.

Earth System Model (ESM) simulations predict that the ocean's O₂ content is sensitive to climate warming, suggesting a significant decline of global O₂ inventory under warming scenarios out to 2100 [Keeling *et al.*, 2010]. While widespread O₂ decline in the extratropical thermocline is a robust projection of the current generation of the ESMs, there are significant differences among models especially in the tropics [Bopp *et al.*, 2013; Cocco *et al.*, 2013]. In a warming climate, increasing seawater temperature decreases oxygen solubility, thereby reducing concentrations assuming all other factors being equal. Furthermore, increased upper ocean stratification associated with surface warming (and increased precipitation and glacier melt) can weaken ventilation, the exchange of well-oxygenated surface waters with the interior ocean. These two mechanisms reinforce one

another to deplete the subsurface oxygen on the centennial timescale [Bopp *et al.*, 2002; Plattner *et al.*, 2002].

Numerous attempts have been made to detect low-frequency variability and long-term trends of subsurface O₂ using historic datasets [Andreev and Baturina, 2006; Emerson *et al.*, 2004; Helm *et al.*, 2011; Johnson and Gruber, 2007; Ono *et al.*, 2001; Sasano *et al.*, 2015; Stendardo and Gruber, 2012; Stramma *et al.*, 2008; van Aken *et al.*, 2011; Whitney *et al.*, 2007; Schmidtko *et al.*, 2017]. Analysis of historic datasets poses significant challenges due to sparse and irregular sampling, making the detection of long-term trends a signal-noise problem [Long *et al.*, 2016]. The global compilation by Garcia *et al.* [2005] revealed significant decadal variability of O₂, AOU and heat content in the upper 100 m for the period of 1955 through 1998. In this time period the magnitude of long-term linear trends of O₂ and AOU are relatively small compared to the decadal-scale fluctuations. Schmidtko *et al.* [2017] included additional data through recent years to calculate the O₂ trends, reporting a significant long-term trend at the rate of $-257.5 \pm 185.1 \text{ TmolO}_2$ (Tmol=10¹²mol) per decade for the upper 1,200m of global oceans, equivalent of about $2 \pm 1.5\%$ loss of the O₂ inventory for the last 50 years. In this study we build on these previous observational efforts; we examine trends in global-scale upper ocean oxygen for the period 1958 through 2015 and examine its relationship with the ocean heat content (OHC) changes.

2. Method

Additional quality control is applied to develop objectively mapped monthly climatologies of O₂ based on the World Ocean Database 2013 [WOD13; Boyer *et al.*, 2013]

at standard depths specified in the dataset. We use an iterative process to construct observationally-based O₂ anomaly fields. Initially, we assemble monthly climatologies using all available data. We then construct the O₂ anomaly fields by subtracting the monthly climatologies from the observed O₂ values. Then we perform the quality control to remove questionable data points that are defined as outliers beyond three times the standard deviation of the anomalies at each point in space. When the questionable data points are removed, we re-calculate the monthly climatologies and repeat the quality control procedure twice in order to minimize questionable data points and biases in climatologies. Anomaly data is binned annually, and the baseline for the anomalies are referenced to the 1950-2015 long-term mean. The resulting O₂ anomaly fields are then objectively mapped onto the global 1° × 1° latitude/longitude grid for each standard depth. A Gaussian weight function is used for the objective mapping with the zonal and meridional length scales of 1,000 km and 500 km, respectively. The data coverage is sparse and uneven, and the sampling density is particularly low in remote regions such as the central subtropical gyres. While the relatively large radius of influence is used to reduce data gaps, it can erroneously blend information across physically separated waters, for example, between marginal seas and open oceans. Regional masks are used for the Mediterranean Sea and the Japan Sea but for the other marginal seas the data from the nearby open ocean can be blended in, which requires caution in the interpretation.

The distribution of O₂ solubility is estimated using temperature and salinity from ocean reanalysis products: the ECMWF Ocean Reanalysis (ORAS4) [*Balmaseda et al.*, 2013] and the Simple Ocean Data Assimilation (SODA version 2.2.4) [*Carton et al.*, 2000]. Rather

than using raw data, we rely on the data assimilation products that are dynamically consistent and are constrained by a suite of hydrographic and satellite observations. For each product, we sample the temperature and salinity at the time and location of the O_2 data points and calculate corresponding oxygen solubility ($O_{2,sat}$) [Garcia and Gordon, 1992]. This calculation allows us to separate O_2 variability into two components: (1) anomalies driven by changes in the solubility of O_2 and (2) anomalies driven by changes in the Apparent Oxygen Utilization ($-AOU = O_2 - O_{2,sat}$). We compute the AOU component by residual, subtracting changes that can be explained by solubility from the total O_2 anomaly. The AOU component reflects the cumulative effect of biological O_2 consumption and the preformed O_2 value of the source waters, thus it depends on ocean circulation, mixing and biochemical processes. Upper ocean heat content is also calculated using the ocean reanalysis products.

Three factors motivate a focus on O_2 variability in the upper ocean. First, the upper ocean O_2 has significant ecological impacts due to proximity to surface ocean habitats. Secondly, upper ocean processes are strongly affected by atmosphere-ocean interactions, thus upper ocean O_2 is likely sensitive to climate variability. Thirdly, the upper ocean is relatively well sampled, enabling more robust analysis with less uncertainty. Even so, significant uncertainty still exists due to the sparse and uneven distribution of data coverage both in time and space. The temporal data coverage is relatively poor in the earliest (1950s) and latest (2010s) part of the time series since some of the latest observations have not yet been included in the database. We examine regional data coverage by counting

the number of years with observations for each $1^\circ \times 1^\circ$ cells of the objectively mapped field (see supplementary figure S1).

With this sparse sampling in mind, we compile the time series of the normalized O_2 inventory in the upper ocean above 1,000 m depth by performing the following calculation,

$$I_{O_2}(t) = \left(\frac{V_{obs}(t)}{V_{tot}} \right)^{-1} \int O'_2(\mathbf{x}, t) dV, \quad (1)$$

where $O'_2(\mathbf{x}, t)$ is the oxygen anomaly, V_{tot} is the total volume of water and $V_{obs}(t)$ is the volume of grid cells filled with O_2 data. The volume integration is based on the same standard depths as the World Ocean Database.

The integral in Eq. (1) is performed with missing data being replaced with zeros, but this produces spurious variability reflecting the year-to-year changes in sampling density.

In order to correct for this bias, the inventory is normalized by the volumetric sampling ratio, $(V_{obs}(t)/V_{tot})$. This correction effectively amplifies the signal when a relatively small volume is sampled, implicitly assuming that the global mean O_2 is correctly represented by the sample mean.

In order to examine the potential errors associated with this method of calculating the global O_2 inventory with relatively sparse observations, we analyze a “large” ensemble of simulations conducted with the Community Earth System Model-Large Ensemble (CESM-LE) project [Kay *et al.*, 2015]. The CESM-LE included 35 ensemble members with ocean biogeochemistry output. The model is spun up to the preindustrial conditions referenced to year 1850 and a single ensemble member was integrated from 1850 to 1920. Additional ensemble members are generated at 1920 by making small ($\mathcal{O}(10^{-14})$ K) perturbations

in the air temperature field and integrated for 181 years from 1920 through 2100, forced by historical forcing through 2005 and by the RCP8.5 forcing from 2006 to 2100. The quality of the O₂ simulation is discussed by *Long et al.* [2016]; briefly, the model simulates a realistic distribution of O₂, but tends to have concentrations and variability (including trends) that are biased low. Even though the model is not perfect, many realizations of the oxygen variability fields allow to evaluate the potential sampling bias in the context of a single mechanistic model.

We calculate the sub-sampled O₂ inventories in the CESM-LE according to the observational sampling pattern including the increased footprint of the data through the objective mapping. The subsampled O₂ inventories are then adjusted according to Eq. (1). We then compare these to the true O₂ inventories for each ensemble member from 1955 to 2015 (figure S2). About 86% of the members (30 out of 35 ensembles) estimated the magnitude of the linear trend to be within the range of -30%+8% of the true trend in the CESM-LE simulations. There is a general tendency that the sub-sampled O₂ inventories underestimate the true global O₂ trend. In 28 out of 35 ensemble members, the linear trend (1958-2015) of sub-sampled O₂ inventories under-estimates the true trend. This indicates that there are regions outside the observational sampling pattern that have stronger trends in O₂ in the CESM-LE simulations. In general, we are encouraged that the existing observations have enough coverage to yield the correct sign of the global trend and the first-order approximation of its magnitude in the context of the CESM-LE.

3. Results

3.1. Global O₂ inventory

The normalized global O₂ inventory is plotted in figure 1a for different depth ranges. Overall the O₂ content increases slightly prior to the mid-1980s, followed by a strong decline after the mid-1980s. This pattern is consistent with the earlier study of *Garcia et al.* [2005] who focused on the upper 100 m inventory for the period of 1955-1998. For the period of 1958 to 2015, the linear trend of upper ocean O₂ inventory (0-1,000m) is $-243 \pm 124 \text{TmolO}_2$ (Tmol= 10^{12} mol) per decade, in agreement with the result of a recent independent study [*Schmidtke et al.*, 2017]. We find that a similar pattern exists throughout the upper 1,000 m of the water column and that the declining trend after the mid-1980s has persisted until recent years. Regression analysis shows that approximately 46% of the variability of the O₂ content occurs above 400 m, and 78% of the variability occurs above 700 m. Figure 1c shows the volumetric sampling ratio, $V_{obs}(t)/V_{tot}$ which is the normalization factor for the O₂ inventory (Eq. 1). The sampling ratio generally exceeds 40% between 1960 and 2010, but most recent years have significantly lower sampling ratio, in part because recent data are not yet included in the database. We expect an increased uncertainty for the most recent years due to sparser sampling; the computed O₂ inventory after 2010 may change significantly when all available data are included in the database.

Figure 1b shows the global OHC based on the ORAS4 dataset. *Balmaseda et al.* [2013] examines the data sources and their calculation of global OHC in detail. There is a slight difference in the OHC time series between the ORAS4 and the WOD13 which shows a long-term positive trend for the entire time period (see https://www.nodc.noaa.gov/OC5/3M_HEAT_CONTENT/). The time evolution global OHC is dominated by the

multi-decadal warming trend with a few episodic cooling events. The cooling episodes matches with the period of volcanic eruptions (El Chichon in 1982 and Mt Pinatubo in 1991) and the period following the 1997-1998 El-Nino event. The normalized O₂ inventory is compared to the OHC time series (Figure 1d). The two time series are significantly correlated according to a *t*-test ($r=-0.86$, 95% CI for 0-1,000 m OHC and O₂).

The regression reveals the relationship between the changes in the OHC and the O₂ inventory. Centennial-scale global warming simulations using ESMs predict that the O₂-heat ratio to be between -5.9 and -6.7 nmol O₂ J⁻¹ [Keeling *et al.*, 2010]. For the normalized O₂ inventory and the OHC above the 1,000 m depth, the regression coefficient is -8.2 ± 0.66 nmol O₂ J⁻¹. The overall agreement in the O₂-heat ratio is remarkable given the uncertainties in the inventory calculation and the potential model errors. A close examination of Figure 1d reveals that the slope of O₂-heat relationship is flatter at shallower depths. The O₂-heat ratio is not uniform spatially; the O₂ inventory appears to be less sensitive to the changes in OHC in the shallower waters, and the ratio increases with depth (supplementary information, Table S1). Above the 100 m depth, the regression coefficient is -1.96 ± 1.27 nmol O₂ J⁻¹, consistent with the expected relationship based on the temperature dependence of solubility [Keeling and Garcia, 2002]. While the linkages between the O₂ content and OHC is not fully understood, the observation suggests that the O₂ inventory in/below the thermocline is significantly more sensitive to the OHC. This may indicate the crucial role played by the ventilation and the circulation changes of the deeper water masses which may reflect the freshening and warming of the water column. This result is consistent with the recent study by Schmidtko *et al.* [2017] that

the O_2 trends above the main thermocline are primarily controlled by the temperature dependence of O_2 solubility, and the AOU component becomes dominant in the deeper waters.

3.2. Global and hemispheric trends in O_2 , $O_{2,sat}$ and AOU

To further investigate the upper ocean O_2 changes, we examine the global and hemispheric area-weighted mean O_2 time series for three depth levels at 100 m, 200 m and 400 m. We include results from the 200 m depth as Figure 2 in the main text; data from the 100 m and 400 m depths are also shown in the supplementary document (Figure S3 and S4). Our calculation of the linear trend and its statistical significance is based on the method of adjusted standard error and adjusted degrees of freedom following *Santer et al.* [2000], wherein a t -test is used to evaluate whether or not the observed linear trend is significantly different from zero. Figure 2ace shows the global and hemispheric time series of O_2 , O_2^{sat} and the negative of AOU at the depth of 200 m. As described above, we compute the negative of AOU as a residual, subtracting the solubility component from the total O_2 anomaly, thus the AOU component captures the O_2 variability not explained by the solubility changes. There are two estimates of O_2^{sat} from the ORAS4 and SODA2.2.4 products which have different temperature/salinity distributions. The two reanalyses agree in the overall magnitude of the $O_{2,sat}$ variability which is much smaller than that of O_2 ; therefore, regardless of the reanalysis product, the AOU component dominates the O_2 variability and so we plot AOU based on ORAS4 only.

The two hemispheres both exhibit multi-decadal O_2 decline but their temporal variabilities are different. It is important to note that the data density of the southern hemisphere

is significantly lower than the northern hemisphere, thus it is more likely influenced by the sampling biases. With this caveat in mind, the global and hemispheric O₂ time series show significant decline after 1980s, which is also evident at 100 m and 400 m depths (see Figures S3 and S4). At 100 m depth, there is a decadal O₂ increase from the 1960s to 1980s for the global and northern hemispheric data as previously identified [Garcia *et al.*, 2005]. Previous investigations of regional O₂ changes have also shown strong O₂ decline in the Pacific basin after 1980s [Deutsch *et al.*, 2011; Czeschel *et al.*, 2012; Stramma *et al.*, 2012; Ito and Deutsch, 2013], which may be related to the reduced ventilation in the Sea of Okhotsk [Ohshima *et al.*, 2014; Nakanowatari *et al.*, 2007].

Figures 2bdf show the global and hemispheric linear trends of O₂ represented as a matrix of trends with varying starting and ending years. The color shading indicates the magnitude of the linear trend and the hatched regions indicate whether the trend is significantly differ from zero (positive or negative) with 95% confidence interval [Santer *et al.*, 2000]. The linear trends are sensitive to the time period of analysis due to the superposition of interannual variability with the multi-decadal trends. Overall the trend matrix is predominantly negative, and the decreasing trends becomes statistically significant with the ending year of 2005 and later. The earlier analysis [Garcia *et al.*, 2005] indeed detected the beginning of post-1980s O₂ decline, despite the relatively narrow time window (1955-1998). Our analysis shows that the negative trend continued to develop during 2000s.

3.3. Spatial pattern of the O₂ trend

Figure 3 shows the maps of the multi-decadal trend over three different depth ranges. There are several regions of intense O₂ decline as noted by earlier investigations such as western subpolar North Pacific [*Ono et al.*, 2001], the Gulf of Alaska [*Whitney et al.*, 2007], equatorial Atlantic and eastern equatorial Pacific [*Stramma et al.*, 2008; *Stramma et al.*, 2012]. The subpolar North Pacific (SPNP) is a relatively well sampled region and exhibits a significant negative trend at all depths as shown by earlier studies [*Ono et al.*, 2001; *Whitney et al.*, 2007]. There are also several regions of O₂ increase such as in the western subtropical North Pacific and eastern subpolar North Atlantic as noticed by previous studies [*Helm et al.*, 2011; *Sasano et al.*, 2015].

Many parts of the global oceans are under-sampled, and the apparent lack of trend may be an artifact of sparse observations in some regions. The open oceans in the extratropical southern hemisphere are poorly sampled in general (Figure S1), and it is possible that the relatively weak trend in the southern hemisphere (Figure 3) may be due to the sparse sampling. In contrast, the Labrador Sea is a relatively well sampled region but the observations do not show a significant trend there. Convective mixing and hydrographic properties of the Labrador Sea are known to exhibit significant interannual and decadal variability, but no significant long-term trend has been observed to date [*Yashayaev*, 2007; *van Aken et al.*, 2011]. Thus, a long-term trend of O₂ is not expected in this region and our result is consistent with these earlier studies.

Finally, we attempt to speculate the potential causes of the observed O₂ changes. Solubility changes only play a secondary role below the thermocline, given the relatively low

variability in the $O_{2,sat}$ component; thus, the O_2 variability is predominantly controlled by AOU changes for the global averages. The changes in AOU can come from many factors; the preformed O_2 value at the location of water mass formation, the rates of biochemical O_2 consumption, the rates of subduction, eddy mixing, and shifts in water mass boundaries. The circulation and eddy stirring can modulate the physical supply of O_2 affecting the regional patterns of O_2 changes [Stramma *et al.*, 2010; Czeschel *et al.*, 2011; Llanillo *et al.*, 2013; Brandt *et al.*, 2015]. Figure 3 shows the contrast between the subpolar and subtropical North Pacific where the O_2 strongly decreases in the subpolar region and it slightly increases in the subtropics. The increase of subtropical O_2 is consistent with the expansion of winter-time isopycnal outcrop where O_2 -rich surface waters subduct into the thermocline [Kwon *et al.*, 2016]. In the subpolar region the thermocline waters are not directly ventilated from the open ocean but the source waters are formed in the marginal seas of the northwestern North Pacific and are strongly influenced by the mixing at the Oyashio front and Kuroshio extension regions [Talley, 1993]. The O_2 decline in the SPNP may reflect the changes in the source regions such as the Sea of Okhotsk or the mixing processes. In the tropical oxygen minimum zones, the ocean climate and circulation variability can shift water masses and alter the rate of nutrient supply to the surface euphotic layer and drive decadal O_2 variability [Deutsch *et al.*, 2011].

4. Discussion

The World Ocean Database 2013 [Boyer *et al.*, 2013] is used to calculate the global O_2 inventory and hemispheric O_2 trends for the period of 1958 to 2015. The distribution of observations is relatively sparse, omitting large regions of the oceans; however, we

demonstrate that this distribution is sufficient to robustly estimate global O₂ trends in the context of an Earth system model simulation. An earlier study [*Garcia et al.*, 2005] with a shorter record period (1955–1998) found little evidence of a long term trend, but our analysis shows that the addition of 17 years of observations has revealed a widespread negative O₂ trend beginning to emerge from the envelope of interannual variability. In conjunction with the O₂ trend, the O₂ solubility and the ocean heat content is examined using temperature and salinity data from ORAS4 [*Balmaseda et al.*, 2013] and SODA2.2.4 [*Carton et al.*, 2000]. Consistent with previous studies, observed O₂ variability is dominated by AOU changes regardless of the dataset used for the temperature and salinity. This indicates that O₂ changes are predominantly driven by changing ocean ventilation and/or biological O₂ consumption. Furthermore, the O₂ inventory is significantly correlated with changes in ocean heat content, particularly for thermocline and deep waters, indicating linkages between the ocean heat uptake and the global AOU increase.

The mechanisms behind the AOU change are not fully understood. In a warming ocean, the surface heating, glacier melt and increased precipitation at high latitudes can increase the ocean stratification, leading to the weakened mixing of O₂-rich surface waters into the thermocline. Earth System Models indeed predict a long term O₂ decline (and increase of AOU as well as ventilation age) on the centennial timescales [*Cocco et al.*, 2013; *Bopp et al.*, 2013; *Long et al.*, 2016]. This mechanism could be at play for the last several decades of O₂ data analyzed here.

The observed O₂ decline is not uniform in space. Relatively strong and widespread O₂ decline is found in the subpolar North Pacific and in the tropics; whereas the subtropical

North Pacific shows a moderate O₂ increase. This pattern has been identified by earlier studies in association with increasing upper ocean stratification [e.g. *Ono et al.*, 2001; *Emerson et al.*, 2004; *Stramma et al.*, 2012], and *Ito et al.* [2016] showed that this pattern may have been caused by the combined effects of natural climate variability and the deposition of polluted dust over the North Pacific Ocean. A recent study [*Long et al.*, 2016] showed that the spatial patterns of O₂ change are similar between the centennial, anthropogenically-forced trend and interannual variability. On this basis, it is possible that the strong O₂ change in the subpolar North Pacific can be caused by either natural climate variability, warming induced long-term change, or some combination of the two.

While climate trends and variability are clearly important drivers of observed O₂ changes, a wider range of processes can contribute to the O₂ changes. For example, *Riebesell et al.* [2007] showed that the C:N utilization ratio of organic matter production in a mesocosm experiment increased under high CO₂ conditions. If this relationship scales globally, the effect could yield larger C:N ratios in sinking organic matter, thereby driving subsurface oxygen declines under high CO₂ conditions (presuming C:O₂ stoichiometry of aerobic respiration remains the same). This effect was included in a modeling study [*Oschlies et al.*, 2008], which showed a 50% increase in the global volume of suboxic (O₂ < 5 μM) waters by 2100 due to increasing C:N ratios in sinking organic matter relative to experiments omitting this effect. In addition to changing C:N utilization ratios, increased exogenous nutrient inputs could drive increased carbon export and oxygen utilization in the interior. *Krishnamurthy et al.* [2010], for instance, simulated anthropogenic enhancements of aerosol nutrient deposition in an Earth system model. Their simulation

showed an increase in the biological productivity in the Pacific basin stimulated by the additional nutrient input from aerosols. Interestingly, the simulated O₂ change in the North Pacific was only moderate in this particular model, and the authors commented that the circulation variability may be more important in driving O₂ variability in this region.

While these perturbations to nutrient cycling could alter the O₂ trends over time, our result reveals a tight relationship between O₂ inventories and OHC. The spatial structure and magnitude of this relationship are consistent with expectations derived from mechanistic models forced under climate warming scenarios. This study owes its existence to the international collaboration through the World Ocean Database Project, and it is crucial to maintain and support the collection and submission of the data. Unfortunately, the spatiotemporal distribution of O₂ observations remains too sparse for definitive conclusions and attribution. However, taken together, the evidence is consistent with anthropogenic warming acting as the primary driver of long-term trends in ocean O₂. The trends we document are suggestive of the effects of warming beginning to supersede natural variability and emerge as a recognizable signal. This merits additional scrutiny over the coming years; if it is the warming signal, we should expect to see continued widespread declines in oceanic O₂. The impacts of ocean deoxygenation on ocean ecosystems may be profound. In this light, it is critical to develop improved understanding of the mechanisms driving trends and variability in the oceanic O₂. The scientific community should work to ensure adequate observing capabilities are maintained; we have an obligation to document and

communicate these impacts of warming, such that society can make informed decisions and understand costs/benefits trade-offs for mitigation.

Acknowledgments. We are thankful for the support from the Scientific Visitor Program of the Climate and Global Dynamics Laboratory at the National Center for Atmospheric Research (NCAR) as this study started while the authors were visiting NCAR during the summer of 2016. NCAR is supported by the National Science Foundation. TI is partially supported by the NSF (OCE-1357373) and NOAA grants (NA16OAR4310173). All datasets supporting the conclusions of this study are available in the public domain as referenced within the paper. Data analysis products used to generate the figures and tables are available from the corresponding author upon request.

References

- Andreev, A. G., and V. I. Baturina (2006), Impacts of tides and atmospheric forcing variability on dissolved oxygen in the subarctic North Pacific, *J. Geophys. Res.*, *111*(C7), C07S10, doi:10.1029/2005JC003103.
- Balmaseda, M. A., K. Mogensen, and A. T. Weaver (2013), Evaluation of the ECMWF ocean reanalysis system ORAS4, *Q. J. R. Meteorol. Soc.*, *139*(674), 1132–1161, doi:10.1002/qj.2063.
- Bopp, L., C. Le Quéré, M. Heimann, A. C. Manning, and P. Monfray (2002), Climate-induced oceanic oxygen fluxes: Implications for the contemporary carbon budget, *Global Biogeochem. Cycles*, *16*, 1022, doi:10.1029/2001GB001445.

Bopp, L., L. Resplandy, J. C. Orr, S. C. Doney, J. P. Dunne, M. Gehlen, P. Halloran, C. Heinze, T. Ilyina, R. Séférian, J. Tjiputra, and M. Vichi (2013), Multiple stressors of ocean ecosystems in the 21st century: projections with CMIP5 models, *Biogeosci.*, *10*, 6225–6245, doi:10.5194/bg-10-6225-2013.

Boyer, T., J. I. Antonov, O. K. Baranova, C. Coleman, H. E. Garcia, A. Grodsky, D. R. Johnson, R. A. Locarnini, A. V. Mishonov, T. O'Brien, C. Paver, J. Reagan, D. Seidov, I. V. Smolyar, and M. M. Zweng (2013), World ocean database 2013, in *NOAA Atlas NESDIS*, vol. 72, edited by S. Levitus and A. Mishonov, p. 209 pp, doi: 10.7289/V5NZ85MT.

Brandt, P., H. W. Bange, D. Banyte, M. Dengler, S.-H. Didwischus, T. Fischer, R. J. Greatbatch, J. Hahn, T. Kanzow, J. Karstensen, A. Körtzinger, G. Krahnemann, S. Schmidtke, L. Stramma, T. Tanhua, and M. Visbeck (2015), On the role of circulation and mixing in the ventilation of oxygen minimum zones with a focus on the eastern tropical north atlantic, *Biogeosci.*, *12*(2), 489–512, doi:10.5194/bg-12-489-2015.

Bretherton, C. S., M. Widmann, V. P. Dymnikov, J. M. Wallace, and I. Blad (1999), The effective number of spatial degrees of freedom of a time-varying field, *Journal of Climate*, *12*(7), 1990–2009, doi:10.1175/1520-0442(1999)012<1990:TENOSD>2.0.CO;2.

Carton, J. A., G. Chepurin, X. Cao, and B. Giese (2000), A Simple Ocean Data Assimilation Analysis of the Global Upper Ocean 1950–95. Part I: Methodology, *J. Phys. Oceanogr.*, *30*(2), 294–309, doi:10.1175/1520-0485(2000)030<0294:ASODAA>2.0.CO;2.

Cocco, V., F. Joos, M. Steinacher, T. L. Frölicher, L. Bopp, J. Dunne, M. Gehlen, C. Heinze, J. Orr, A. Oschlies, B. Schneider, J. Segschneider, and J. Tjiputra (2013),

Oxygen and indicators of stress for marine life in multi-model global warming projections, *Biogeosciences*, *10*, 1849–1868, doi:10.5194/bg-10-1849-2013.

Czeschel, R., L. Stramma, F. U. Schwarzkopf, B. S. Giese, A. Funk, and J. Karstensen (2011), Middepth circulation of the eastern tropical south pacific and its link to the oxygen minimum zone, *J. Geophys. Res.*, *116*(C1), C01015, doi:10.1029/2010JC006565.

Czeschel, R., L. Stramma, and G. C. Johnson (2012), Oxygen decreases and variability in the eastern equatorial pacific, *Journal of Geophysical Research: Oceans*, *117*(C11), n/a–n/a, doi:10.1029/2012JC008043, c11019.

Deutsch, C., H. Brix, T. Ito, H. Frenzel, and L. Thompson (2011), Climate-forced variability of ocean hypoxia, *Science*, *333*(6040), 336–339, doi:10.1126/science.1202422.

Emerson, S., Y. Watanabe, T. Ono, and S. Mecking (2004), Temporal Trends in Apparent Oxygen Utilization in the Upper Pycnocline of the North Pacific: 1980–2000, *J. Oceanogr.*, *60*(1), 139–147, doi:10.1023/B:JOCE.0000038323.62130.a0.

Garcia, H. E., and L. I. Gordon (1992), Oxygen solubility in seawater: Better fitting equations, *Limnology and Oceanography*, *37*(6), 1307–1312, doi:10.4319/lo.1992.37.6.1307.

Garcia, H. E., T. P. Boyer, S. Levitus, R. A. Locarnini, and J. Antonov (2005), On the variability of dissolved oxygen and apparent oxygen utilization content for the upper world ocean: 1955 to 1998, *Geophys. Res. Lett.*, *32*, L09604, doi:10.1029/2004GL022286.

Gruber, N. (2011), Warming up, turning sour, losing breath: ocean biogeochemistry under global change, *Philos. Trans. Roy. Soc.*, *369*, 1980–1996, doi:10.1098/rsta.2011.0003.

Helm, K. P., N. L. Bindoff, and J. A. Church (2011), Observed decreases in oxygen content of the global ocean, *Geophys. Res. Lett.*, *38*, L23602, doi:10.1029/2011GL049513.

Ito, T., and C. Deutsch (2013), Variability of the oxygen minimum zone in the tropical north pacific during the late twentieth century, *Global Biogeochemical Cycles*, *27*(4), 1119–1128, doi:10.1002/2013GB004567.

Ito, T., A. Nenes, M. S. Johnson, N. Meskhidze, and C. Deutsch (2016), Acceleration of oxygen decline in the tropical pacific over the past decades by aerosol pollutants, *Nature Geosci*, *9*(6), 443–447, doi:10.1038/ngeo2717<http://www.nature.com/ngeo/journal/v9/n6/abs/ngeo2717.html#supplementary-information>.

Johnson, G. C., and N. Gruber (2007), Decadal water mass variations along 20°W in the Northeastern Atlantic Ocean, *Prog. Oceanogr.*, *73*, 277–295, doi:10.1016/j.pocean.2006.03.022.

Kay, J. E., C. Deser, A. Phillips, A. Mai, C. Hannay, G. Strand, J. M. Arblaster, S. C. Bates, G. Danabasoglu, J. Edwards, M. Holland, P. Kushner, J. F. Lamarque, D. Lawrence, K. Lindsay, A. Middleton, E. Munoz, R. Neale, K. Oleson, L. Polvani, and M. Vertenstein (2015), The community earth system model (cesm) large ensemble project a community resource for studying climate change in the presence of internal climate variability, *Bull. Amer. Meteor. Soc.*, *96*(8), 1333–1349, doi:10.1175/bams-d-13-00255.1.

Keeling, R. F., and H. E. Garcia (2002), The change in oceanic O₂ inventory associated with recent global warming, *Proc. Natl. Acad. Sci. U.S.A.*, *99*(12), 7848–7853, doi:10.1073/pnas.122154899.

Keeling, R. F., A. Körtzinger, and N. Gruber (2010), Ocean Deoxygenation in a Warming World, *Ann. Rev. of Mar. Sci.*, *2*, 199–229, doi:10.1146/annurev.marine.010908.163855.

Krishnamurthy, A., J. K. Moore, N. Mahowald, C. Luo, and C. S. Zender (2010), Impacts of atmospheric nutrient inputs on marine biogeochemistry, *J. Geophys. Res.*, *115*(G1), doi:10.1029/2009JG001115.

Kwon, E. Y., C. Deutsch, S.-P. Xie, S. Schmidtko, and Y.-K. Cho (2016), The north pacific oxygen uptake rates over the past half century, *J. Clim.*, *29*(1), 61–76, doi: 10.1175/JCLI-D-14-00157.1.

Llanillo, P. J., J. Karstensen, J. L. Pelegrí, and L. Stramma (2013), Physical and biogeochemical forcing of oxygen and nitrate changes during el nino/el viejo and la nina/la vieja upper-ocean phases in the tropical eastern south pacific along 86w, *Biogeosci.*, *10*(10), 6339–6355, doi:10.5194/bg-10-6339-2013.

Long, M. C., C. A. Deutsch, and T. Ito (2016), Finding forced trends in oceanic oxygen, *Global Biogeochem. Cycles*, *30*, doi:10.1002/2015GB005310.

Nakanowatari, T., K. I. Ohshima, and M. Wakatsuchi (2007), Warming and oxygen decrease of intermediate water in the northwestern north pacific, originating from the sea of okhotsk, 1955–2004, *Geophysical Research Letters*, *34*(4), n/a–n/a, doi: 10.1029/2006GL028243, 104602.

Ohshima, K. I., T. Nakanowatari, S. Riser, Y. Volkov, and M. Wakatsuchi (2014), Freshening and dense shelf water reduction in the okhotsk sea linked with sea ice decline, *Progress in Oceanography*, *126*, 71 – 79, doi:http://dx.doi.org/10.1016/j.pocean.2014.04.020, biogeochemical and physical processes in the Sea of Okhotsk and the linkages

to the Pacific Ocean.

Ono, T., T. Midorikawa, Y. W. Watanabe, K. Tadokoro, and T. Saino (2001), Temporal increases of phosphate and apparent oxygen utilization in the subsurface waters of western subarctic Pacific from 1968 to 1998, *Geophys. Res. Lett.*, *28*(17), 3285–3288, doi:10.1029/2001GL012948.

Oschlies, A., K. G. Schulz, U. Riebesell, and A. Schmittner (2008), Simulated 21st century's increase in oceanic suboxia by co₂-enhanced biotic carbon export, *Global Biogeochemical Cycles*, *22*(4), n/a–n/a, doi:10.1029/2007GB003147, gB4008.

Plattner, G.-K., F. Joos, and T. F. Stocker (2002), Revision of the global carbon budget due to changing air-sea oxygen fluxes, *Global Biogeochem. Cycles*, *16*, 1096, doi:10.1029/2001GB001746.

Riebesell, U., K. G. Schulz, R. G. J. Bellerby, M. Botros, P. Fritsche, M. Meyerhofer, C. Neill, G. Nondal, A. Oschlies, J. Wohlers, and E. Zollner (2007), Enhanced biological carbon consumption in a high co₂ ocean, *Nature*, *450*(7169), 545–U10, doi:10.1038/nature06267.

Santer, B. D., T. M. L. Wigley, J. S. Boyle, D. J. Gaffen, J. J. Hnilo, D. Nychka, D. E. Parker, and K. E. Taylor (2000), Statistical significance of trends and trend differences in layer-average atmospheric temperature time series, *J. Geophys. Res.*, *105*(D6), 7337–7356, doi:10.1029/1999JD901105.

Sasano, D., Y. Takatani, N. Kosugi, T. Nakano, T. Midorikawa, and M. Ishii (2015), Multidecadal trends of oxygen and their controlling factors in the western North Pacific, *Global Biogeochem. Cycles*, *29*, 935–956, doi:10.1002/2014GB005065.

- Schmidtko, S., L. Stramma, and M. Visbeck (2017), Decline in global oceanic oxygen content during the past five decades, *Nature*, *542*(7641), 335–339, doi:10.1038/nature21399.
- Stendardo, I., and N. Gruber (2012), Oxygen trends over five decades in the North Atlantic, *J. Geophys. Res.*, *117*, C11004, doi:10.1029/2012JC007909.
- Stramma, L., G. C. Johnson, J. Sprintall, and V. Mohrholz (2008), Expanding Oxygen-Minimum Zones in the Tropical Oceans, *Science*, *320*, 655–658, doi:10.1126/science.1153847.
- Stramma, L., G. C. Johnson, E. Firing, and S. Schmidtko (2010), Eastern pacific oxygen minimum zones: Supply paths and multidecadal changes, *J. Geophys. Res.*, *115*(C9), C09011, doi:10.1029/2009JC005976.
- Stramma, L., A. Oschlies, and S. Schmidtko (2012), Mismatch between observed and modeled trends in dissolved upper-ocean oxygen over the last 50 yr, *Biogeosciences*, *9*(10), 4045–4057, doi:10.5194/bg-9-4045-2012.
- Talley, L. D. (1993), Distribution and formation of north pacific intermediate water, *Journal of Physical Oceanography*, *23*(3), 517–537, doi:10.1175/1520-0485(1993)023<0517:DAFONP>2.0.CO;2.
- van Aken, H. M., M. Femke de Jong, and I. Yashayaev (2011), Decadal and multi-decadal variability of Labrador Sea Water in the north-western North Atlantic Ocean derived from tracer distributions: Heat budget, ventilation, and advection, *Deep Sea Res.*, *58*, 505–523, doi:10.1016/j.dsr.2011.02.008.
- Whitney, F. A., H. J. Freeland, and M. Robert (2007), Persistently declining oxygen levels in the interior waters of the eastern subarctic Pacific, *Prog. Oceanogr.*, *75*, 179–199, doi:

10.1016/j.pocean.2007.08.007.

Yashayaev, I. (2007), Hydrographic changes in the labrador sea, 1960-2005 (vol 73, pg242, 2007), *Progress in Oceanography*, 75(4), 857–859, doi:10.1016/j.pocean.2007.09.001.

Accepted Article

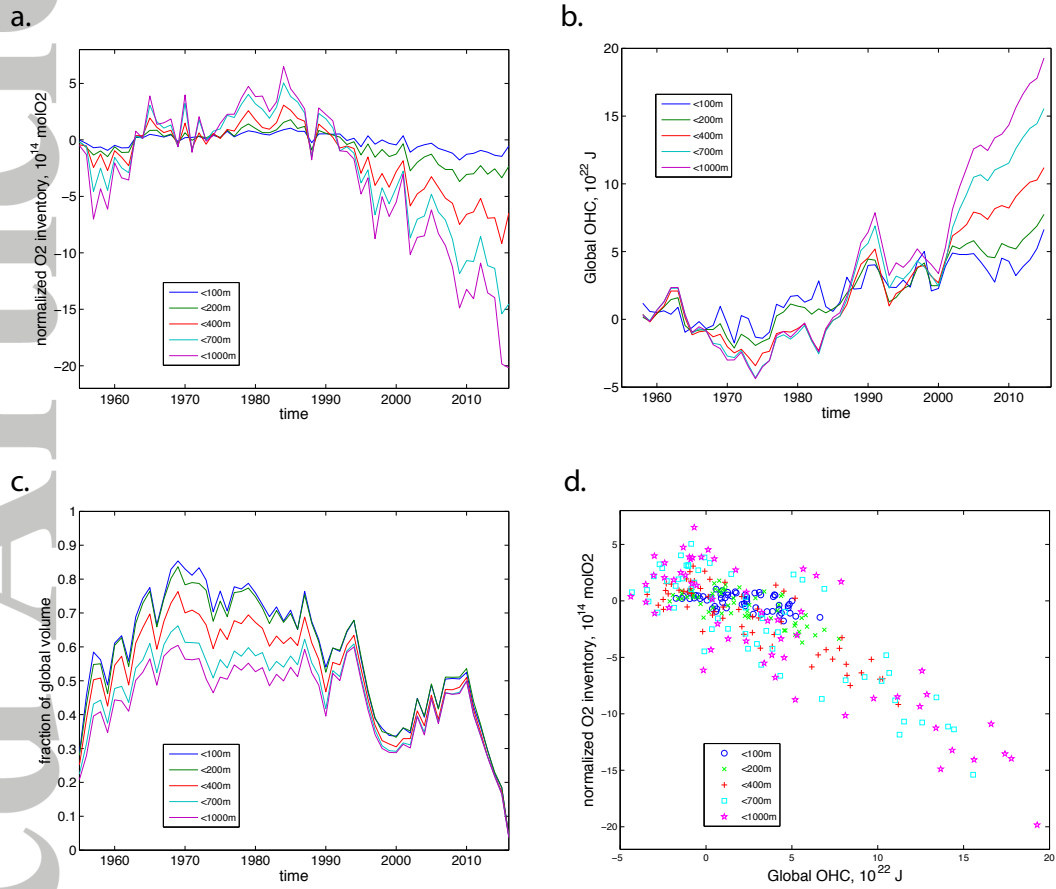


Figure 1. (a) Normalized O₂ inventory above the depths of 100m (blue), 200m (green), 400m (red), 700m (teal) and 1,000m (purple). (b) Global OHC based on the ORAS4 dataset. The color coding is the same as (a) indicating the vertical range of integration. (c) Volumetric sampling density measured as the fraction of grid cells filled with data. (d) The scatter diagram of the normalized O₂ inventory versus OHC. The significance testing of the correlation is performed according to the definition of the effective sample size according to *Bretherton et al.* [1999].

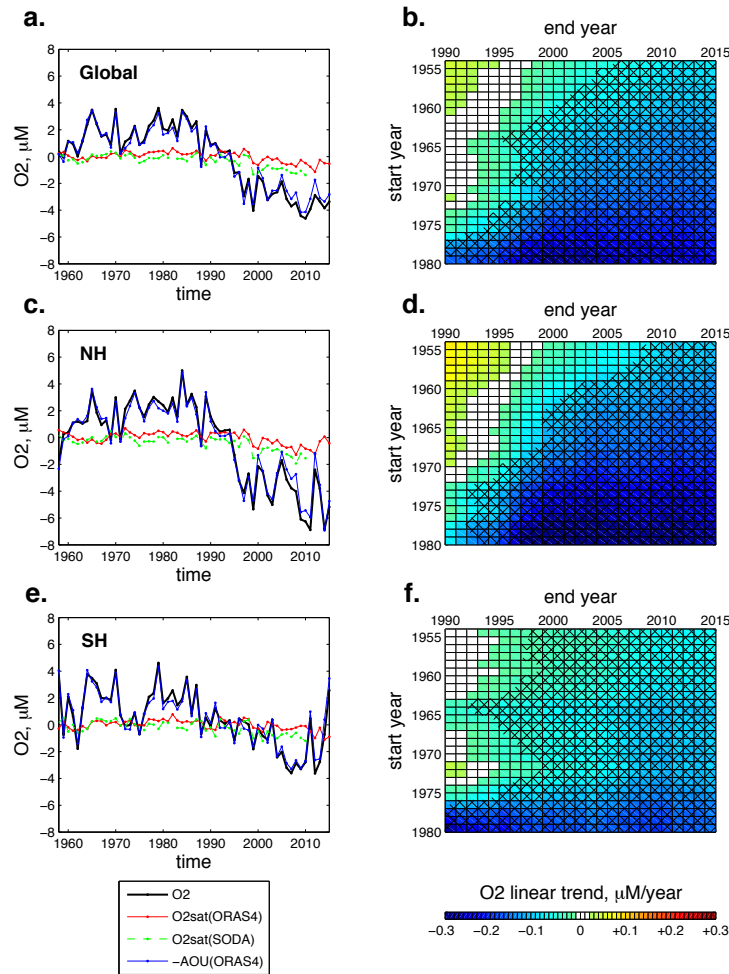


Figure 2. (a) Global O₂ time series at the depth of 200m. Data points are weighted by the cosine of latitude. Black is O₂, Red and Green are O₂ saturation based on ORAS4 and SODA2.2.4 respectively. Blue is (-1) x AOU. (b) Trend matrix is formed by taking linear trend of O₂ with different starting and ending years. Color shading shows the magnitude of the trend. Hatching is applied for positive/negative definite trends with 95% CI using the method of adjusted standard error and adjusted degree of freedom following Santer et al. [2000]. (c,d) the same as (a,b) but for the northern hemispheric data points only. (e,f) the same as (a,b) but for the southern hemispheric data points only.

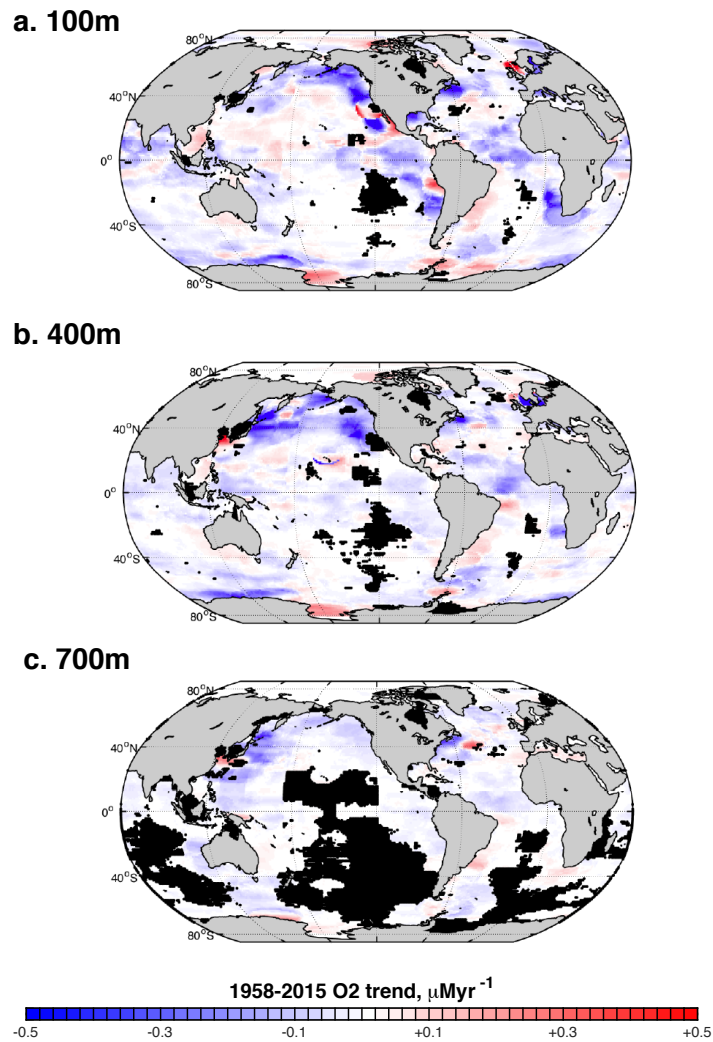


Figure 3. (a) Global map of the linear trend of O₂ time series at the depth of 100m. We plot the linear trend for the grid cells where the effective sample size (N_{eff}) is greater than 20. (b) same as (a) but at the depth of 400m. (c) same as (a) but at the depth of 700m. We indicate the regions where there are insufficient data ($N_{eff} < 20$) by black dots.